

T-3162

RESISTIVITY AND THERMOPOWER OF AMORPHOUS  
ANTIMONY AND TELLURIUM FILMS

by

Bennet L. Abramoff

ProQuest Number: 10782774

All rights reserved

INFORMATION TO ALL USERS

The quality of this reproduction is dependent upon the quality of the copy submitted.

In the unlikely event that the author did not send a complete manuscript and there are missing pages, these will be noted. Also, if material had to be removed, a note will indicate the deletion.



ProQuest 10782774

Published by ProQuest LLC (2018). Copyright of the Dissertation is held by the Author.

All rights reserved.

This work is protected against unauthorized copying under Title 17, United States Code  
Microform Edition © ProQuest LLC.

ProQuest LLC.  
789 East Eisenhower Parkway  
P.O. Box 1346  
Ann Arbor, MI 48106 – 1346

T-3162

A thesis submitted to the faculty and the Board of Trustees of the Colorado School of Mines in partial fulfillment of the requirements for the degree of Master of Science (Physics).

Golden, Colorado

Date 11/21/85

Signed: Bennet L. Abramoff  
Bennet L. Abramoff

Approved: J.U. Trefny  
Dr. J.U. Trefny  
Thesis Advisor

Golden, Colorado

Date 11/21/85

COLORED SCHOOL OF MINES  
GOLDEN, COLORADO

F.D. Schowengerdt  
Dr. F.D. Schowengerdt  
Head of Physics Department

## ABSTRACT

A technique for preparing uniform amorphous antimony and tellurium films by evaporation onto a cold substrate was developed. The resistivity and thermopower of amorphous tellurium, annealed polycrystalline tellurium, amorphous antimony, and annealed polycrystalline antimony films were measured from 120K - 320K. The thermopowers of uniform-amorphous antimony and of amorphous tellurium films are reported here for the first time. The thermopower of amorphous antimony was found to be large and n-type and that of amorphous tellurium was found to be large and p-type. The results for the resistivity of amorphous antimony agree well with those previously reported while those for amorphous tellurium do not. The behavior of both the resistivity and the thermopower of the amorphous films was compared to models for extended state conduction, variable range hopping, nearest neighbor hopping, and small polaron conduction, but it was impossible to conclusively decide which of these mechanisms actually took place.

## TABLE OF CONTENTS

	<u>Page</u>
ABSTRACT .....	iii
TABLE OF CONTENTS .....	iv
LIST OF FIGURES .....	v
LIST OF TABLES .....	vi
ACKNOWLEDGEMENTS .....	vii
I. INTRODUCTION .....	1
II. EXPERIMENTAL PROCEDURE .....	4
A. Sample Preparation .....	4
B. Measurement Procedure .....	9
1) Measurement Sequence .....	9
2) Temperature Measurement .....	12
3) Manual Measurement of Resistance .....	13
4) Automatic Measurement of Resistance .....	14
5) Manual Measurement of Thermopower .....	15
6) Automatic Measurement of Thermopower .....	17
7) Measurement Frequency .....	18
8) Resistivity Measurement .....	18
III. THEORY .....	20
IV. RESULTS AND DISCUSSION .....	31
A. Antimony .....	31
B. Tellurium .....	40
V. SUMMARY .....	61
REFERENCES CITED .....	63

## LIST OF FIGURES

<u>No.</u>		<u>Page</u>
1.	Deposition System .....	5
2.	Sample Holder .....	6
3.	Thermocouple Leads .....	11
4.	Resistivity of Antimony vs. $10^3/T$ .....	32
5.	Resistivity of Antimony vs. $T^{-1/4}$ .....	33
6.	Thermopower of Antimony vs. $10^3/T$ .....	36
7.	Resistivity of Annealed Antimony vs. $10^3/T$ .....	39
8.	Thermopower of Annealed Antimony vs. $T$ .....	39
9.	Total Resistivity of Tellurium vs. $T^{-1/4}$ .....	41
10.	Resistivity of Tellurium vs. $T^{-1/4}$ .....	42
11.	Resistivity of Tellurium vs. $10^3/T$ .....	43
12.	Thermopower of Te 3 vs. $DT$ .....	47
13.	Thermopower of Te 2 vs. $T$ .....	48
14.	Thermopower of Te 3 vs. $T$ .....	48
15.	Thermopower of Te 2 vs. $10^3/T$ .....	50
16.	Thermopower of Te 3 vs. $10^3/T$ .....	50
17.	Resistivity of Annealed Tellurium vs. $10^3/T$ .....	52
18.	Thermopower of Annealed Tellurium vs. $10^3/T$ .....	54
19.	Electron Micrograph of Annealed Te 2 .....	56
20.	Electron Micrograph of Te 4 .....	58

LIST OF TABLES

<u>No.</u>		<u>Page</u>
1.	DT, thickness, $T_{min}$ , $T_{max}$ , $T_{cry}$ , and $R_{sh}$ of tellurium .....	44

ACKNOWLEDGEMENTS

I give special thanks to my thesis advisor, Dr. John U. Trefny. I also acknowledge the help of electron microscope operator Robert McGrue, electronics specialists Rex Rideout, John Udd, and Ken Winans, instrument maker Jack Kintner, Professor Don L. Williamson, students Doug Cook, Dave Fobare, Jim Madsen, Robert Philbin, and Tim Vaughn, and thesis committee members Dr. Mark A. Passler and Dr. F. Richard Yeatts.

## I. INTRODUCTION

The study of amorphous semiconductors is new compared to the study of crystalline semiconducting materials. Amorphous silicon has been of particular interest because it is more economical to produce than crystalline silicon, and can be manipulated by such processes as hydrogenation to have electrical qualities similar to those of its popular, but more costly, crystalline counterpart.

Anderson and Mott developed some of the early theoretical models of amorphous semiconductors. Anderson predicted that there are localized states in these materials. Mott predicted that for amorphous semiconductors with a high density of localized states, electrical conduction at low temperature takes place by hopping.<sup>(1)</sup> Experimental tests have since confirmed the existence of hopping in amorphous elements such as antimony, arsenic, germanium, silicon, and in various alloys as well.<sup>(2)</sup> Very few thermopower measurements have been made and there has been less experimental support of Mott's prediction for thermopower when electrical conduction takes place by hopping.

The author's predecessor, D.S. Peters, submitted a thesis in which he reported the resistivity and thermopower of amorphous antimony and tellurium films on mylar

substrates.<sup>(3)</sup> Due to mylar's highly flexible quality, only the very ends of the sample were in good thermal contact with the cold reservoir. The films appeared shiny near the ends and less lustrous in the middle. An amorphous material's resistivity is a few orders of magnitude greater than that of the corresponding crystalline semiconductor. The resistivity of amorphous tellurium reported by D.S. Peters was as small as the resistivity of crystalline tellurium, and a few orders of magnitude smaller than what A.M. Phale reported for amorphous tellurium films.<sup>(4)</sup> This indicates that the tellurium films measured by D.S. Peters were crystalline. The resistivity of amorphous antimony films reported by D.S. Peters was only about one order of magnitude greater than the resistivity of crystalline antimony, and several orders of magnitude smaller than what J.J. Hauser reported for amorphous antimony films.<sup>(2)</sup> Later, D. Cook, the author's colleague, prepared antimony films in the same manner as D.S. Peters. He found that the resistivity of the center of the film was as small as that of crystal antimony. These results indicated that only the very ends of the antimony films made by D.S. Peters were amorphous. Clearly, there was a need to produce uniform amorphous films.

The main purpose of this research project was to develop a technique of preparing uniform amorphous tellurium films and to make order of magnitude measurements of the thermopower and resistivity of these films. This task was accomplished by inquiring how to clean substrates, designing and constructing a new substrate holder, and acquiring and learning how to operate an electrometer. These new techniques and equipment represent refinements on the techniques developed and equipment assembled by D.S. Peters.

## II. EXPERIMENTAL PROCEDURE

### A. Sample Preparation.

Figure 1 shows the deposition system. Not shown are the AC power supply for the tungsten filament, the vacuum monitor for the thermocouple vacuum gauge, and the ultrahigh vacuum monitor for the ionization tube. Figure 2 is an upside down exploded diagram of the sample holder. Not shown is the silicone cement between the probe holder, heat sinks, mylar, and copper probes. Also not shown is the double sided cellophane tape between the foam pads and the copper plate. Substrates of 1.0" x 1.0" x 0.032" corning 7059 glass were used. The substrates were cleaned ultrasonically in a trichloroethylene bath and then rinsed with acetone, methanol, and distilled water, in that order. The substrate was held with tongs and rinsed repeatedly with each solution using a squirt bottle, while being held above the tongs so the rinsing solution would flow from the substrate to the tongs, preventing contamination from the tongs or the hand.

Next, three substrates were laid in a line on the copper plate. On either side of this line, 0.2" thick aluminum strips were held with double stick cellophane tape to the copper plate to keep the substrates from sliding out

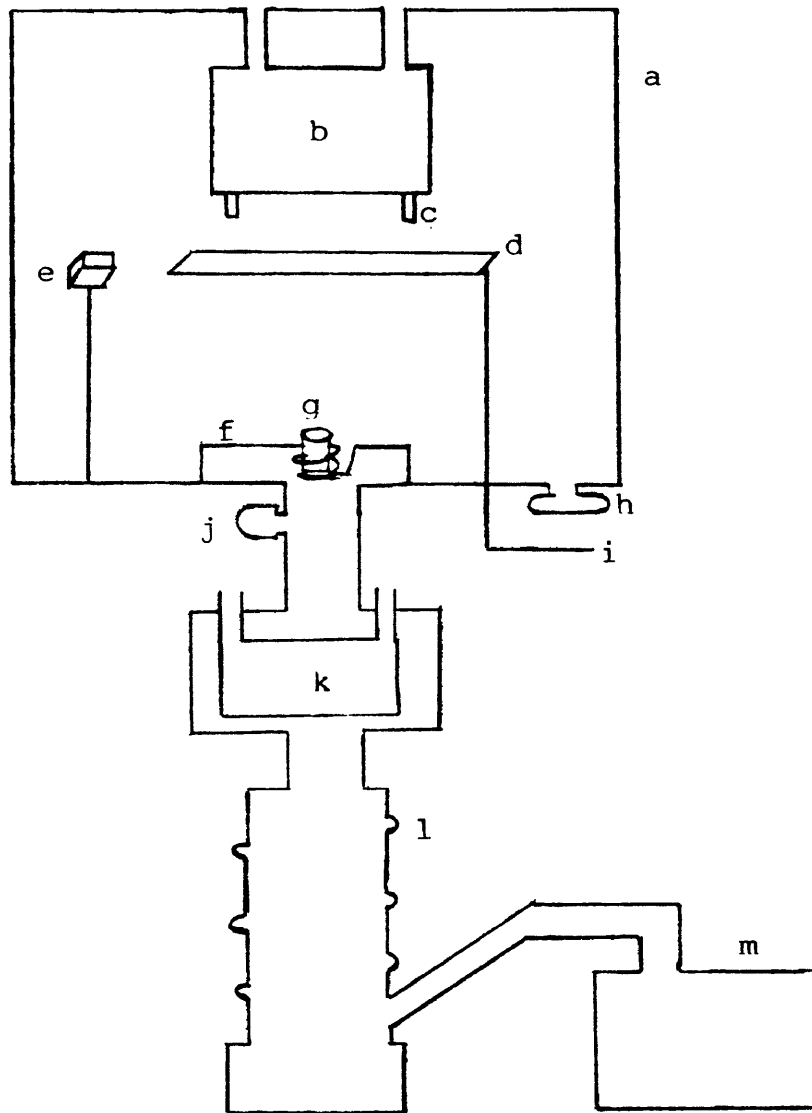


Figure 1. Deposition System. (a - vacuum chamber, b - top cold reservoir, c - lug, d - shutter, e - quartz crystal, f - tungsten filament, g - alumina crucible, h - ionization tube, i - shutter control level, j - thermocouple vacuum probe, k - bottom cold reservoir, l - diffusion pump, m - mechanical pump.)

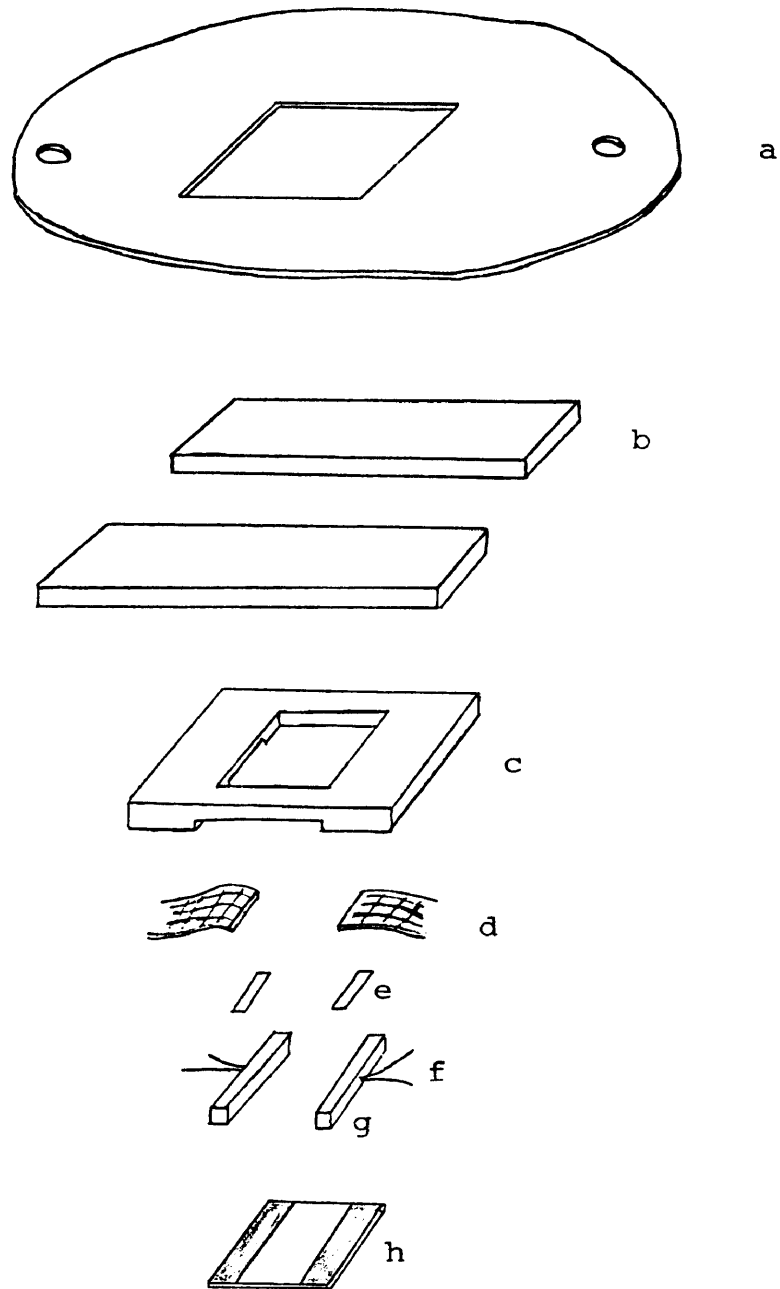


Figure 2. Sample Holder. (a - copper plate, b - foam pad, c - probe holder, d - heat sink, e - mylar, f - thermocouple, g - copper probe, h - substrate with pre-evaporated tabs.)

of position. A 0.505" wide, 0.2" thick aluminum strip was placed lengthwise over the center of the substrates and taped to the copper plate. The copper plate was then screwed to the lugs under the cold reservoir, substrate side down. For substrates to be used for Te samples, the tabs were made of Te, and likewise, for substrates to be used for Sb samples, the tabs were made of Sb. The proper evaporation charge was placed in the alumina crucible. The Te charge consisted of 99.9998% pure pieces, 2mm or smaller. The Sb charge consisted of 99.9999% pure 1 mm shot.

Once the evaporation chamber was sealed, evacuation would begin by turning on the mechanical pump. After the pressure dropped to below 50 millitorr, as measured by the thermocouple vacuum gauge, the bottom cold reservoir was filled with liquid nitrogen and the diffusion pump was turned on. When the pressure dropped to the  $10^{-5}$  torr range, as measured by the ionization vacuum gauge, the top reservoir was filled with liquid nitrogen. After the reservoir had fully cooled, evaporation could begin. (Cooling the top reservoir was an optional step for making tabs, but a necessary step for making samples. Tabs were often co-evaporated with samples for expediency. Temperature measurement will be discussed later.) The voltage from the AC power supply to the filament was slowly raised. The

thickness of the deposited film is directly related to, and was estimated from, the frequency change displayed on the quartz crystal monitor. When the rate of deposition reached about three angstroms/second, the shutter was opened and the voltage of the power supply was no longer raised. Deposition continued at this rate until the desired thickness was achieved. During deposition, the substrate temperature was typically about 140K and the pressure about  $3.0 \times 10^{-5}$  torr.

Next, the sample was evaporated onto a substrate with pre-evaporated tabs. The substrate was gently clamped to the cold reservoir. The clamping force was adjusted by changing the distance of the copper plate relative to the cold reservoir, and was just great enough to provide good electrical contact between the copper probes and the pre-evaporated tabs. This distance was determined by placing a substrate whose surface was coated with an antimony film in the sample holder, and moving the copper plate towards the cold reservoir until the resistance of the film measured would not substantially decrease upon further increase of the clamping force. (Resistance measurement will be discussed below.)

The substrate holder design evolved by trial and error. Both the heat sinks and the gentle clamping force were found to be necessary. Without heat sinks, the

substrates were not cold enough for the films to be deposited amorphous. With too firm a clamping force the films would crack. Each of the two heat sinks was screwed directly to the cold reservoir at a lug. To insure that good electrical contact could be provided with only a small clamping force, the probes were each milled, polished with a series of sandpaper of decreasing grit size, lapped with a paste of alumina powder and water on a surface of window glass, and cemented in a coplanar position onto the probe holder. Also, the cold reservoir was milled and polished.

B. Measurement Procedure.

1) Measurement Sequence.

After the sample was deposited, the diffusion pump was turned off. The top and cold reservoirs were then allowed to run out of liquid nitrogen as it boiled off. Once the top trap ran out of liquid nitrogen, it and the substrate would slowly warm to room temperature. The sample's temperature, resistance, and thermopower were measured periodically as it warmed. The sample, which was deposited amorphous due to the substrate's cold temperature, would abruptly and irreversibly change to a polycrystalline film before reaching room temperature. Tellurium and antimony samples had different crystallization temperatures, but both

were below room temperature. After reaching room temperature, the sample was cooled back to cryogenic temperature and the measurement process was repeated on the annealed crystalline samples.

Soldered into each of the copper probes was a constantan-chromel thermocouple. Taped to one of the two heat sinks was a 20 ohm resistor. As soon as the sample was deposited, a potential difference of three volts was applied across this resistor causing a temperature gradient across the sample. Figure 3 is a schematic diagram of the two thermocouples and the sample.

In-situ measurements were made with two different sets of measurement instruments which were connected to the two thermocouples. Measurements of amorphous antimony, crystalline antimony, and crystalline tellurium films, whose resistance ranged from  $10^0$  -  $10^6$  ohms, were made with an automatic data acquisition system consisting of a Rockwell-Aime 65 Microcomputer, custom built switch box, and a Keithley 195 Digital Multimeter. Measurements of amorphous tellurium films, whose resistance ranged from  $10^9$  -  $10^{11}$  ohms, were made manually with a Keithley 602 Electrometer.

After the sample was removed from the vacuum chamber, its thickness was measured with a stylus gauge. The width and length of the sample were measured with a vernier

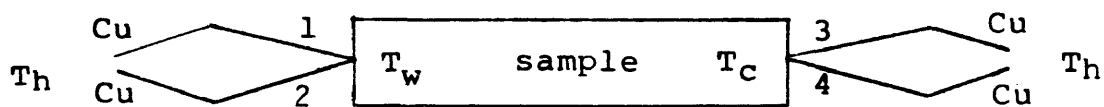


Figure 3.  $T_h$  - room temperature,  $T_c$  - temperature of the sample's cold end,  $T_w$  - temperature of the sample's warm end, Cu - copper leads, 1 and 3 - constantan leads, 2 and 4 - chromel leads.

caliper. The surface structures of the films were studied with a Rigaku automated x-ray diffraction spectrometer and by scanning electron microscopy.

## 2) Temperature Measurement.

The voltage across each constantan-chromel thermocouple was used to determine the temperature of the thermocouple junction, with the calibration table provided by the manufacturer of the thermocouple leads, Omega. Thus the voltage across leads 1 and 2,  $V_{12}$ , determined  $T_w$  and the voltage across leads 3 and 4,  $V_{34}$ , determined  $T_c$ .

The Omega table is calculated for  $T_h = 0^\circ\text{C}$ , while  $T_h$  for this experiment, as measured by an ordinary thermometer, was actually  $28^\circ\text{C}$ . The chart gives the voltage for a constantan-chromel thermocouple at  $28^\circ\text{C}$  to be  $1.678\text{ mV}$ , and this correction must be first added to  $V_{12}$  and  $V_{34}$  to yield  $V_{12}(T_h = 0^\circ\text{C})$  and  $V_{34}(T_h = 0^\circ\text{C})$ . As an example for  $V_{12} = -7.21\text{ mV}$  and  $V_{34} = -8.31\text{ mV}$ ,

$$V_{12}(T_h = 0^\circ\text{C}) = -7.21\text{ mV} + 1.678\text{ mV} = -5.532\text{ mV}$$

$$V_{34}(T_h = 0^\circ\text{C}) = -8.31\text{ mV} + 1.678\text{ mV} = -6.632\text{ mV}$$

The values for  $T_w$  and  $T_c$  were then interpolated from the Omega table. In this example,  $T_w$  and  $T_c$  were  $-107^\circ\text{C}$  and

-133°C respectively. The average temperature in Kelvin degrees was then 153K, and the temperature difference was 26K.

The above sample calculation was for a manual measurement. The microcomputer of the automatic data acquisition system could not store the entire Omega table, and it calculated temperatures from a cubic least squares parameterization instead.

### 3) Manual Measurement of Resistance.

The resistance of an amorphous tellurium film was manually measured. Before the film was evaporated, the shunt resistance was measured. Resistance measurements were made across leads 1 and 4 with the electrometer at the  $10^9$  ohm position. The shunt resistance did not vary much with temperature and was assumed constant. The equation relating the shunt resistance,  $R_{sh}$ , the total resistance,  $R_t$ , and the resistance of the sample,  $R$ , is simply the equation for resistors in parallel:

$$\frac{1}{R_t} = \frac{1}{R_{sh}} + \frac{1}{R} .$$

Writing  $R$  explicitly gives

$$R = \left( \frac{1}{R_t} - \frac{1}{R_{sh}} \right)^{-1} .$$

For example, for  $R_{sh} = 9.2 \times 10^9 \Omega$  and  $R_t = 5.3 \times 10^9 \Omega$ ,  $R$  is calculated to be  $12.5 \times 10^9 \Omega$ .

#### 4) Automatic Measurement of Resistance.

The resistance of amorphous antimony, crystalline antimony, and crystalline tellurium films was measured automatically. To measure the resistance of a sample using the automatic data acquisition system, a current of  $1 \mu\text{A}$  was run from lead 2 to lead 4 and the voltage,  $V_{13}(+)$ , across leads 1 and 3 was measured. The current was then reversed and the voltage,  $V_{13}(-)$  was measured. In this manner, the resistance of the sample was measured without having to consider the resistance of the leads or the thermopower of the sample in the calculations. The two voltage equations are

$$V_{13}(+) = V_{13} \text{ (current off) } + 1 \times 10^{-6} \text{ amp} \times R$$

$$V_{13}(-) = V_{13} \text{ (current off) } - 1 \times 10^{-6} \text{ amp} \times R.$$

Solving for  $R$  yields

$$R = \frac{V_{13}(+) - V_{13}(-)}{2 \times 10^{-6}} .$$

A sample calculation for  $V_{13}(+) = .193709$  volts and  $V_{13}(-) = -.193983$  volts gives

$$R = 1.94 \times 10^5 \Omega .$$

5) Manual Measurement of Thermopower.

For the amorphous tellurium films, which were manually measured, the current from lead 4 to lead 1,  $I$ , was measured with the electrometer at the  $10^{-11}$  amp position. This current was the short circuit current generated by the thermoemf of the sample. The thermopower of the sample,  $S$ , was determined from  $I$ ,  $R$ , the thermopower of the constantan lead,  $S_{con}$ , and the thermopower of the chromel lead,  $S_{chr}$ , by the equation

$$IR = S_{con}(T_h - T_w) + S(T_w - T_c) + S_{chr}(T_c - T_h).$$

This expression is from the general equation  $\vec{E} = \rho \vec{J} + S \nabla T$ , discussed later, with the approximation that  $E = 0$  for a current measurement. Writing  $S$  explicitly yields

$$S = \frac{IR - S_{con}(T_h - T_w) - S_{chr}(T_c - T_h)}{T_w - T_c} .$$

Using the same apparatus as the author, R. Philbin measured the temperature coefficients of  $S_{\text{con}}$  and  $S_{\text{chr}}$  with a standard sample of gold wire and produced the following cubic least square fit equations:

$$S_{\text{chr}} = (8.204 \times 10^{-7} T^3 - 8.157 \times 10^{-4} T^2 + .2562 T - 3.210) \mu\text{V/K}$$

$$S_{\text{con}} = (-4.880 \times 10^{-7} T^3 + 4.206 \times 10^{-4} T^2 - .2704 T - 1.660) \mu\text{V/K} .$$

As an example, the sample whose manually measured temperature and resistance has been described in the previous calculations, had a short circuit current of 5.6 pA. For this sample,

$$S_{\text{chr}} = 19.858 \mu\text{V/K}$$

$$S_{\text{con}} = 35.004 \mu\text{V/K}$$

and thus,

$$\begin{aligned}
 S &= (2.66 + .18 + .12) \times 10^3 \mu\text{V/K} \\
 &= 2.96 \times 10^3 \mu\text{V/K} .
 \end{aligned}$$

6) Automatic Measurement Thermopower.

Using the automatic data acquisition system, the thermopower of amorphous antimony, crystalline antimony, and crystalline tellurium films was determined by measuring the voltage across leads 1 and 3,  $V_{13}$ , and the voltage across leads 2 and 4,  $V_{24}$ . Using the general equation  $\vec{E} = \rho\vec{J} - S\vec{\nabla}T$  again, but with current equal to zero under the open circuit condition of a voltage measurement gives

$$\begin{aligned}
 V_{13} &= S_{\text{con}} (T_h - T_w) + S(T_w - T_c) + S_{\text{con}}(T_c - T_h) \\
 V_{24} &= S_{\text{chr}} (T_h - T_w) + S(T_w - T_c) + S_{\text{chr}}(T_c - T_h) .
 \end{aligned}$$

Calling  $S$  from the top equation  $S_{13}$  and  $S$  from the bottom equation  $S_{24}$ , cancelling terms, and writing  $S$  explicitly yields

$$\begin{aligned}
 S_{13} &= \frac{V_{13}}{DT} + S_{\text{con}} \\
 S_{24} &= \frac{V_{24}}{DT} + S_{\text{chr}} .
 \end{aligned}$$

$S$  is then the average of these two values:

$$S = \frac{S_{13} + S_{24}}{2} .$$

#### 7) Measurement Frequency.

For automatic data acquisition, a set of in situ measurements was taken every time  $V_{12}$  would change by 100 microvolts, which was about every 2 degrees. Manual measurements could not be taken frequently because of the long time constant of the measurement of resistance, and the even longer time constant of the measurement of the current across the very high resistance samples. A set of measurements was taken every 15 minutes. The procedure was to record  $I$  after 12 minutes,  $R_t$  after 3 minutes, and then  $V_{12}$  and  $V_{34}$ .

#### 8) Resistivity Measurement.

In order to allow room for error when mounting the substrate, the distance between the pre-evaporated tabs, .0128m, was less than the distance between the copper probes, .0170m. The latter distance was considered the length of the crystalline films. However, since the resistance of the crystalline tabs was negligible compared to the resistance of the amorphous films, the former distance was considered the length of the amorphous films.

The resistivity,  $\rho$ , was calculated with the equation

$$\rho = \frac{\text{area}}{\text{length}} R .$$

For an amorphous film with  $R = 12.5 \times 10^9$  ohms, thickness =  $4780 \times 10^{-10}\text{m}$ , and width =  $.0255\text{m}$ :

$$\begin{aligned} \rho &= \frac{(4780 \times 10^{-10}\text{m})(.0255\text{m})}{.0128\text{m}} 12.5 \times 10^9 \Omega \\ &= 1.19 \times 10^4 \Omega\text{-m} \end{aligned}$$

## III. THEORY

The general expression for electric current density is

$$\vec{J} = n q \vec{v},$$

where  $\vec{J}$  is the net charge transported per area per time,  $n$  is the volume density of the charge carriers,  $q$  is the charge of a carrier, and  $\vec{v}$  is the time averaged or drift velocity of the charge carriers.

The electric current density due to an applied electric field is

$$\vec{J} = \sigma \vec{E}$$

where the electrical conductivity is

$$\sigma = \frac{nq^2\tau}{m} = 1/\rho .$$

The multiplicative inverse of the conductivity,  $\rho$ , is called the resistivity.  $\tau$  is the average time a carrier is accelerated by the field before being scattered. The electrical conductivity can also be expressed as

$$\sigma = nq\mu,$$

where  $\mu$ , the mobility is

$$\mu = |\vec{v}| / |\vec{E}|$$

The two usual kinds of charge carriers in materials are electrons and holes. They have opposite, but equal, charge. An electron has a charge of  $-e$ , where  $e$  is a positive quantity, and a hole has a charge of  $+e$ . The drift velocities of electrons and holes due to an electric field are also opposite. Thus, in a general equation for electric current density, the currents of electrons and holes due to an electric field add constructively. The electrical conductivity in terms of these two separate contributions is

$$\sigma = |e| (n_e \mu_e + n_h \mu_h),$$

where the mobilities are both positive by convention. The subscripts  $e$  and  $h$  refer to electrons and holes respectively.

In a true metal, all electrons are described by extended states. When an electric field is applied, many of the electrons are accelerated until they are scattered at

lattice defects or impurities. The effective carrier concentration is on the order of magnitude of  $10^{22}/\text{cm}^3$  and is independent of temperature. The number of impurity atoms and lattice defects such as vacancies and dislocations are temperature independent. However, the periodicity of the lattice is also distorted by thermal oscillations. The mean lifetime of a carrier due to scattering by thermal distortion varies as  $1/T$ , where  $T$  is the absolute temperature. Above cryogenic temperatures, this scattering mechanism dominates and the conductivity varies as  $1/T$ .<sup>(5)</sup>

In a semimetal, the valence and conduction bands overlap slightly. At zero temperature, the valence band is full and the non-overlapping portion of the conduction band is empty. At increased temperature, electrons are thermally excited to available conduction states. Every electron excited in this manner leaves behind a hole carrier in the valence band. Carrier concentrations, and thus electrical conductivities of semimetals, are a few orders of magnitude lower than true metals. In semimetals, the carrier concentration as well as the mobility are temperature dependent and the temperature dependence of electrical conductivity is not as easy to predict as for true metals.

Antimony is a semimetal. For polycrystalline antimony the carrier concentration linearly increases with  $T$  and the

mobility linearly decreases with  $T$ .<sup>(6)</sup> A plot of  $\ln \rho$  vs.  $T$  is flat for films of about  $500 \text{ \AA}$ , is linear with increasingly positive slope as thickness becomes smaller, and is linear with increasingly negative slope as the thickness increases from  $500 \text{ \AA}$  to  $2000 \text{ \AA}$ .<sup>(7)</sup>

In semiconductors, there is a gap between the valence and conduction bands. The energy of the top of the valence band is  $E_V$  and the energy of the bottom of the conduction band is  $E_C$ . The energy gap is then

$$E_g = E_C - E_V.$$

In intrinsic semiconductors, all electrons in the conduction band have been thermally excited from the valence band. Thus, there are an equal number of holes and electrons. A semiconductor with equal numbers of holes and electrons is called an intrinsic semiconductor. The electrical conductivity for an intrinsic semiconductor is

$$\sigma = 2|e| \left( \frac{2\pi kT}{h^2} \right)^{3/2} m_e m_h e^{-E_g/2kT} (\mu_e + \mu_h),$$

where  $k$  is the Boltzmann constant and  $h$  is Planck's constant. The mobility in most semiconductors varies as  $T^{-3/2}$  so the electrical conductivity is proportional to  $e^{-E_g/2kT}$ .

Impurity atoms can donate or accept electrons, upsetting the balance of holes and electrons. If the impurity atoms are donors, then the Fermi energy,  $E_f$ , the energy at which the probability of a state being occupied is  $1/2$  according to the Fermi-Dirac distribution function, is moved from the intrinsic semiconductor's Fermi energy at the band gap mid point towards  $E_c$ . The electrical conductivity is then proportional to  $e^{-(E_c - E_f)/kT}$ . If the impurity atoms are acceptors, then  $E_f$  is moved towards  $E_v$  and the electrical conductivity is proportional to  $e^{-(E_f - E_v)/kT}$ . (5) It has been observed that polycrystalline tellurium films are extrinsic below about 100K and intrinsic above about 200K. (8)

Amorphous solids do not have the long range periodicity of crystalline solids. They have bond angles and interatomic spacings very close to those occurring in a crystalline material of the same chemical composition. However, these quantities vary slightly from atom to atom so that an amorphous solid has a short range order like that of a crystal, but no long range order at all. Anderson showed that solutions for electron states in a semiconductor with either slightly varying potentials or interatomic spacings include not only extended states with the same band gap as for the corresponding crystal but also localized states within the band gap.

Trapping and recombination, processes which have been ignored so far in this discussion, severely limit extended state conduction in amorphous solids with a high density of localized states. Carriers are trapped and released at localized states near the band edges, and electron-hole pairs recombine at localized states towards the middle of the gap. Mott showed theoretically that a form of electrical conduction other than extended state conduction, hopping, may take place in amorphous semiconductors. Although the electrical conductivity due to hopping is much smaller than the electrical conductivity due to extended state conduction in a crystalline semiconductor, it may nevertheless be the dominant form of electrical conduction in an amorphous semiconductor.

Mott's hopping theory is as follows. The wave function for an electron in a localized state decays exponentially with distance. The probability that it is a distance,  $R$ , away from the physical center of its localized state is proportional to  $e^{-2\alpha R}$ , where  $\alpha$  is a positive coefficient. Most of the states below  $E_f$  are filled and most above are empty. It is possible for an electron just below  $E_f$  to be excited to a state just above  $E_f$ . If the energy difference between these two states is  $W$ , then this energy must be provided by a phonon whose energy is at least  $W$ . The

probability that a phonon has an energy of  $W$  is proportional to  $e^{-W/kT}$ . If the phonon frequency,  $\nu_{ph}$ , is taken to be the hopping attempt frequency, then the probability of a hop per second is

$$\nu_{ph} e^{-(2\alpha R - W/kT)}$$

At low temperatures, phonon energies are low and many of the hops will be to states more than one site away where a localized state with low  $W$  may be found. As temperature increases, so do phonon energies and the hopping rate increases, especially to nearby sites. Eventually, as temperature is increased still further, hopping is almost exclusively to nearest neighbor sites. Nearest neighbor hopping also occurs if  $\alpha$  is large. In the temperature range where the average hopping distance decreases as temperature increases, conduction is called variable range hopping. In this range  $\sigma$  is proportional to  $e^{-(T_0/T)^{1/4}}$  where

$$T_0 = 24\alpha^3/\pi N(E_f)k,$$

and  $N(E_f)$  is the density of states at  $E_f$ . Electrical conduction in both amorphous antimony and tellurium films below room temperature has been observed to be by variable range

hopping.(2,4) For nearest neighbor hopping,  $\sigma$  is proportional to  $e^{-W/kT}$ .(1)

An applied electric field is not the only possible source of an electric current. An applied temperature gradient also causes a flow of charge. The carriers at the warm end of a sample diffuse to the cold end of the sample. This is because the carriers at the warm end have a higher speed than the carriers at the cold end. Both holes and electrons diffuse towards the cold end.

Holes and electrons have opposite charge sign but the same direction of travel, due to a thermal gradient. Therefore, the hole and electron currents due to a temperature gradient add destructively, rather than constructively, as they do when they are caused by an electric field. If the hole and electron carrier densities and/or mobilities are unequal, there will be a net flow of one type of charge due to a temperature gradient towards the cold end. If the net flow is due to holes then the material is called p-type, and if the net flow is due to electrons the material is called n-type. This net current density is proportional to  $\vec{\nabla}T$ . The electric current density due to both an electric field and a temperature gradient is commonly expressed as

$$\vec{J} = \sigma \vec{E} - \sigma S \vec{\nabla}T ,$$

where  $S$  is the thermopower. Writing  $\vec{E}$  explicitly gives

$$\vec{E} = \rho \vec{J} + S \vec{\nabla} T .$$

If a sample is electrically insulated, so that  $\vec{J} = 0$ , then

$$\vec{S} = \frac{|\vec{E}|}{|\vec{\nabla} T|} .$$

This last sentence is the definition of the thermopower. It follows from this definition that  $S$  is positive for p-type materials and negative for n-type materials. The voltage generated by a sample in this open circuit measurement is called the thermoemf.

For a true metal the expression for thermopower is

$$S = - \frac{\pi^2 k^2 T}{3e} \left( \frac{\partial \ln \sigma}{\partial \epsilon} \right)_{E_f} ,$$

where  $\epsilon$  is the energy of an electron. Since the expression in the parentheses is independent of temperature and usually positive,  $S$  is negative and proportional to  $T$ .<sup>(9)</sup> The thermopower of polycrystalline antimony films is positive and proportional to  $T$ .<sup>(7)</sup>

The thermopower due to holes in a semiconductor is

$$S_h = \frac{k}{e} \left( \frac{E_f - E_v}{kT} + A \right)$$

and the thermopower due to electrons in a semiconductor is

$$S_e = \frac{-k}{e} \left( \frac{E_c - E_f}{kT} + B \right) .$$

A and B are constants which vary from 0 to 4 and depend on the scattering mechanism. The energy difference in each expression corresponds to the thermal energy transported by the carrier. If a material is strongly n or p-type, then its thermopower is expressed by  $S_e$  or  $S_n$  respectively. The general expression for thermopower in a semiconductor is

$$S = \frac{\sigma_h S_h + \sigma_e S_e}{\sigma_h + \sigma_e} .$$

In amorphous semiconductors, the above equation holds unless conduction is by variable range hopping. If conduction is by hopping, then the thermopower is theoretically predicted as

$$S = \frac{1}{2} \frac{k}{e} \frac{W^2}{kT} \left( \frac{d \ln n}{d\epsilon} \right)_{E_f} .$$

This expression predicts a very small value for  $S$  since  $W$ , which represents the average thermal energy transported by a carrier, is small. There has been little experimental confirmation of this prediction.<sup>(1)</sup>

In a semiconductor, a carrier trapped in a localized state distorts the surrounding structure and can strongly interact with a phonon forming a polaron. In a crystalline semiconductor whose charge carriers are polarons, as temperature is increased above zero, the polarons become freed and the resistivity decreases until it reaches a minimum. Then, as temperature is increased further, resistivity increases as the polarons are increasingly scattered by phonons. As the temperature reaches one half the Debye temperature, the resistivity is a maximum. Above one half the Debye temperature, electrical conductivity follows the usual temperature dependence for extended state conduction except for one small difference next described.

The amount of energy by which the trapped electron's energy is lowered in the presence of the distorted lattice is called the polarization energy,  $W_p$ . The activation energy for electrical conductivity is raised by  $W_p/2$ . However, the activation energy for thermopower is unchanged. An energy difference of this kind of about .1eV has been observed in several amorphous semiconductors, and is considered evidence for conduction by polarons in them.<sup>(1)</sup>

## IV. RESULTS AND DISCUSSION

A. Antimony.

Figure 4 shows the resistivity of antimony vs.  $10^3/T$ . The thickness of the film was  $3230 \text{ \AA}$ . As viewed by the naked eye the annealed film appeared shiny and uniform. Between  $-30^\circ\text{C}$  and  $-25^\circ\text{C}$  the resistivity dropped three orders of magnitude as the film crystallized. In the low temperature region and especially towards the crystallization point, the plot is quite linear with positive slope. The  $1/T$  temperature dependence of resistivity is evidence of transport by extended state conduction or nearest neighbor hopping. The best fit straight line shown was plotted and its slope determined by the CSM computer library's least square best fit routine. (This was the same method used on all best fit lines shown in subsequent figures.) The activation energy or nearest neighbor hopping energy, as determined by the best fit, is  $.16\text{eV}$ . It is impossible to decide from this plot if conduction is by nearest neighbor hopping or by extended state conduction or by both, because the magnitude of resistivity and the slope of the plot are reasonable values for either mechanism.

Figure 5 is a plot of resistivity of antimony vs.  $T^{-1/4}$ . The raw data used for this plot were the same data

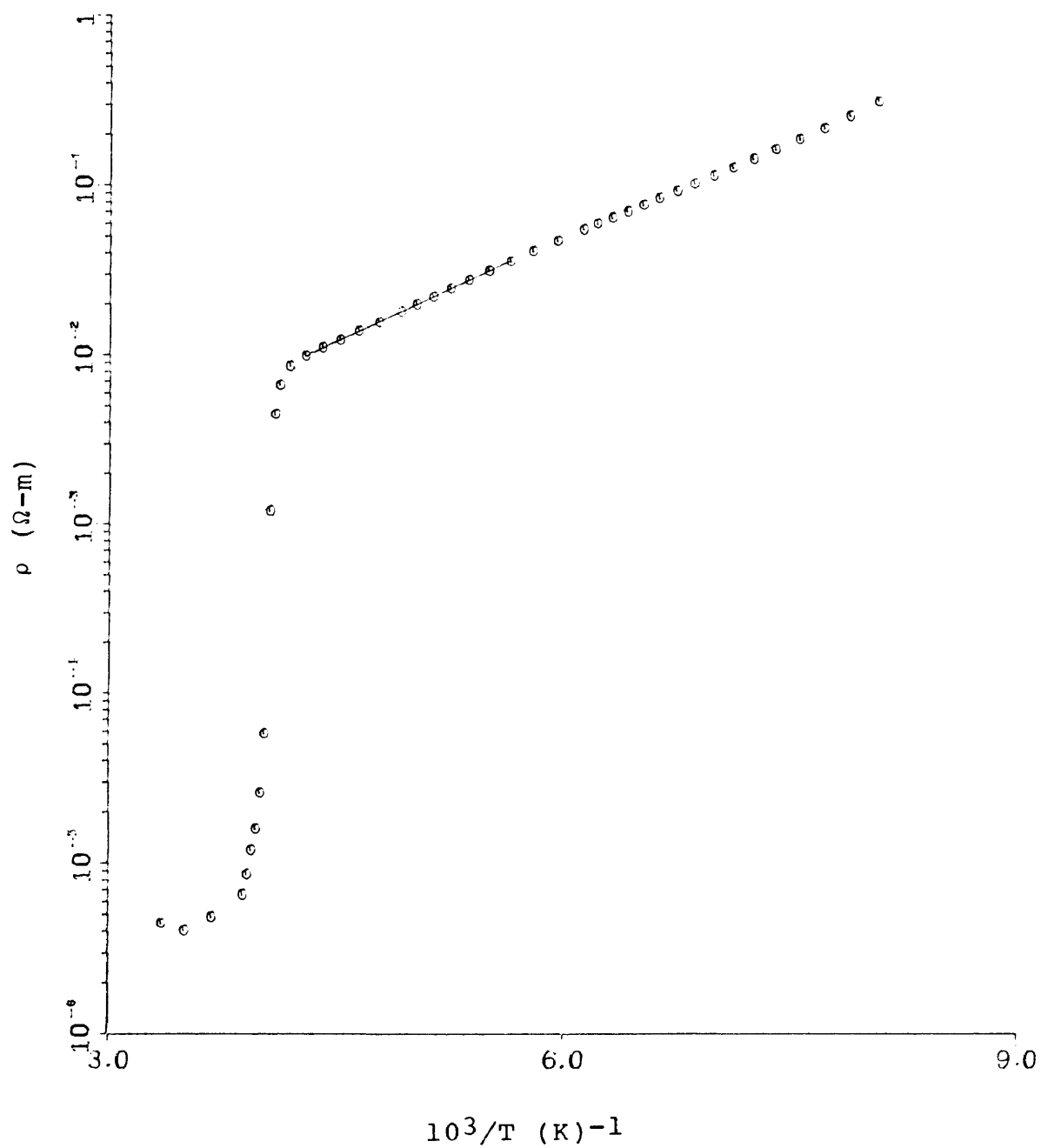


Figure 4. Resistivity of antimony vs.  $10^3/T$ .

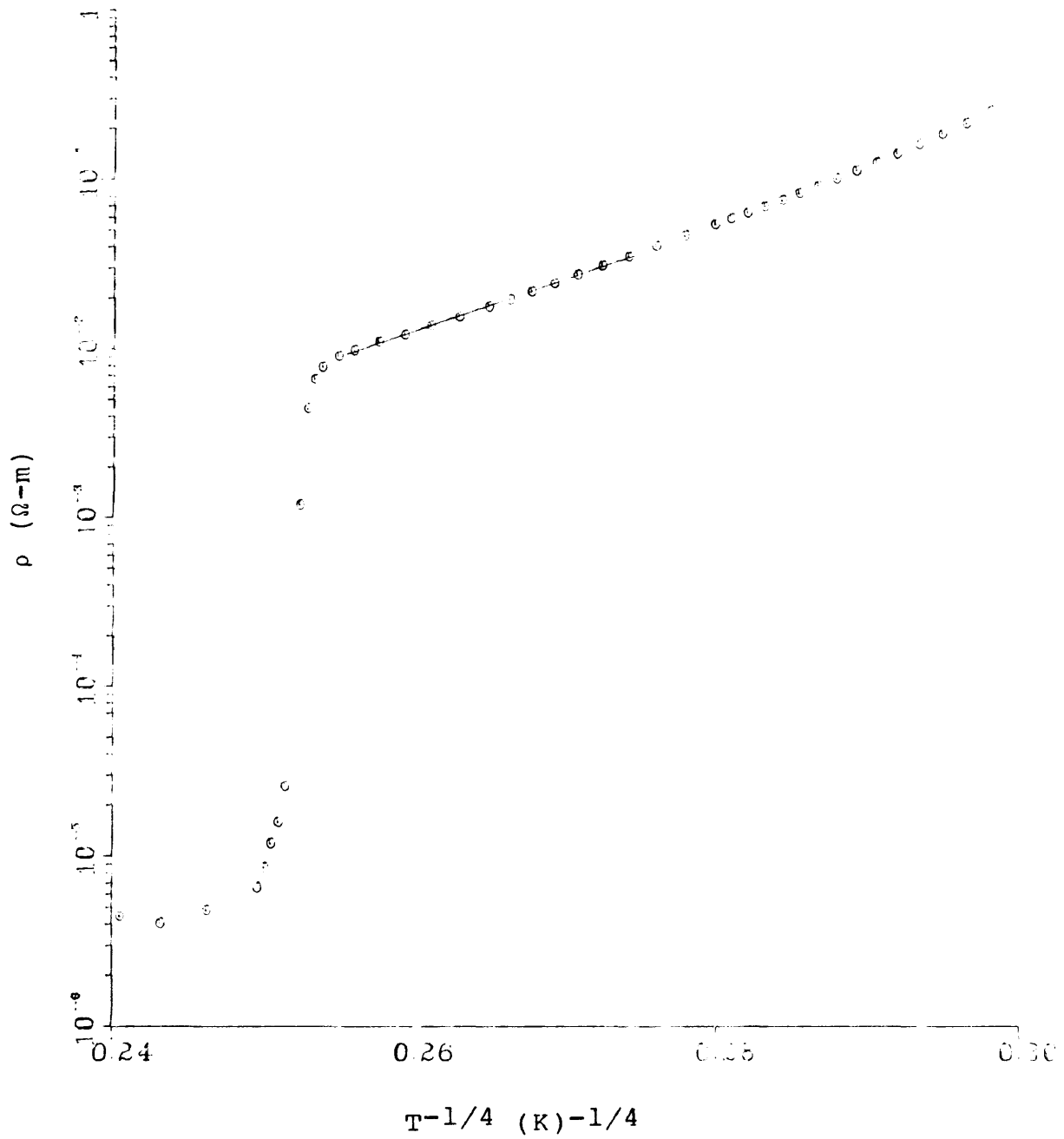


Figure 5. Resistivity of antimony vs.  $T^{-1/4}$ .

that were used for Figure 4. The low temperature region of the plot is also, but not quite as, linear as that of Figure 4. The  $T^{-1/4}$  dependence of resistivity is evidence of variable range hopping. The value of  $T_0$  is  $24 \times 10^6$  K.

Although the  $1/T$  dependence is more closely linear than the  $T^{-1/4}$  dependence, variable range hopping cannot be ruled out because of the uncertainty of the temperature measurements. Two different tests were made with the goal of calibrating the thermocouples, but the results were inconsistent and are not used in these plots. In the first test, the thermocouples were immersed in liquid nitrogen. For this test,  $T$  and  $DT$  were 78K and -1K respectively. The actual temperature of liquid nitrogen at the mile high elevation of our laboratory is 75K. In the second test,  $T$  and  $DT$  were measured with the probes held firmly against the cold reservoir, from cryogenic to room temperature without the heater on. This test was run twice with the positions of the heat sinks altered in the second run. The values of  $DT$  were -9K and -4K at  $T = 100$ K. These values of  $DT$  decreased linearly with temperature until they reached 0K at room temperature.

The results of Figures 4 and 5 differ from what was reported by D.S. Peters<sup>(2)</sup> and J.J. Hauser<sup>(3)</sup>. Peters reported  $T_0$  as 1 to  $2 \times 10^6$  K, a crystallization temperature

of  $-38^{\circ}\text{C}$ , and resistivities of one order of magnitude less than those reported here. Hauser reported  $T_0$  as  $7 \times 10^6$  K, a crystallization temperature of  $-3^{\circ}\text{C}$ , and resistivities within one order of magnitude of those reported here.

Possible explanations for some of these differences are as follows. Since  $N(E_f)$  is proportional to  $1/T_0$ , then the high value of  $T_0$  reported here represents films with a low density of localized states. Peters' films had low resistivity because only a small portion of his films were actually amorphous. The films were amorphous at the very ends and crystalline in the middle. The high density of localized states in Peters' films was due to defects at their crystalline-amorphous interface. Hauser's films were deposited at a rate 100 times greater than the rate of deposition of the films reported here. The high density of states in Hauser's films are caused by the high rate of deposition. Hauser also reported  $T_0 = 20 \times 10^6$  K for antimony films sputtered at  $3 \text{ \AA}^0/\text{sec}$ . These values of  $T_0$  and deposition rate agree closely with those reported here. However, Hauser's sputtered films had a crystallization temperature of  $40^{\circ}\text{C}$  which he conjectured was due to the incorporation of Argon.

Figure 6 is a plot of the thermopower of antimony vs.  $10^3/T$ . In the low temperature region, the thermopower is

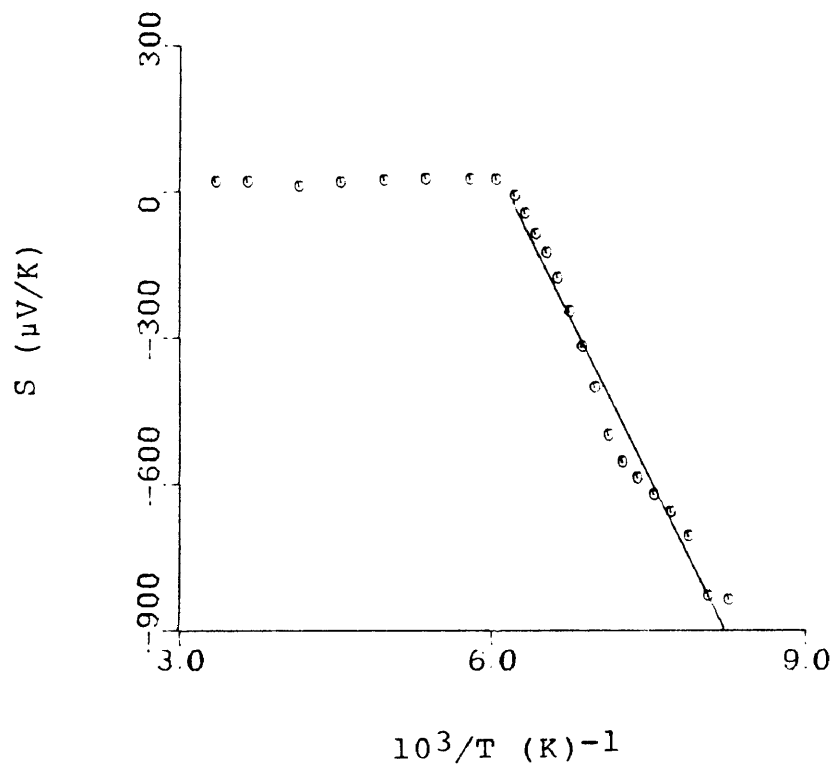


Figure 6. Thermopower of antimony vs.  $10^3/T$ .

negative and the plot is linear with a negative slope. Assuming this negative slope is determined by the equation for  $S_h$  gives  $E_c - E_f = .43\text{eV}$ . This gap is  $.27\text{eV}$  larger than the gap determined from the resistivity plot, rather the smaller as predicted by the small polaron hopping theory. The thermopower reaches about  $+20 \mu\text{V/K}$  at  $165\text{K}$ , well below the crystallization temperature, and then varies very gradually with temperature.  $S$  increases to a maximum of  $28 \mu\text{V/K}$  at  $172\text{K}$  and then decreases to a minimum of  $12 \mu\text{V/K}$  at  $241\text{K}$  ( $-32^\circ\text{C}$ ), just before crystallization. Assuming  $S = S_h$  between  $172\text{K}$  and  $241\text{K}$  gives  $E_f - E_v = .012\text{eV}$ . This is  $.15\text{eV}$  smaller than the activation energy from the resistivity plot and thus the high temperature thermopower of amorphous antimony agrees well with theoretical predictions for small polaron hopping. This agreement could easily be just a coincidence. The sharp changes in the behavior of the thermopower are not reflected in the plot of resistivity as might be expected, except for a small kink in the resistivity plot which might be due to the error in temperature measurement.

The thermopower of amorphous antimony films reported by D.S. Peters is quite different. He found  $S$  was  $+120 \mu\text{V/K}$  at low temperatures, decreased with temperature until it reached  $-20 \mu\text{V/K}$  at  $200\text{K}$ , and increased to about  $0$  at

crystallization. It is possible that the negative thermopower reported here is due to the incorporation of oxygen. D.S. Peters' films were evaporated at a pressure that was one tenth the pressure at which the films reported were evaporated. There is evidence that only with relatively high pressure during evaporation is the thermopower of amorphous germanium films negative.<sup>(1)</sup>

Figures 7 and 8 are of the annealed polycrystalline antimony film. Figure 7 is a plot of the resistivity of the annealed film vs. temperature. The plot indicates the film is semiconductor-like with an energy gap of .028eV. This plot most resembles the results by A. Boyer et al. for their 200 Å film. That film had a negative, although linear, temperature dependence. The difference between these results does not necessarily represent a contradiction, since the films of Boyer et al. were evaporated at room temperature.

Figure 8 is a plot of the thermopower of the annealed antimony film versus temperature. The positive linear temperature dependence indicates the film is metal-like, in contradiction to the results of Figure 7. This figure agrees closely with the plot by Boyer et al. for their 200 Å film, which is shown in Figure 8 by the dashed line, but not as well with the plots for their thicker films which had greater slopes and magnitudes of thermopower.<sup>(7)</sup>

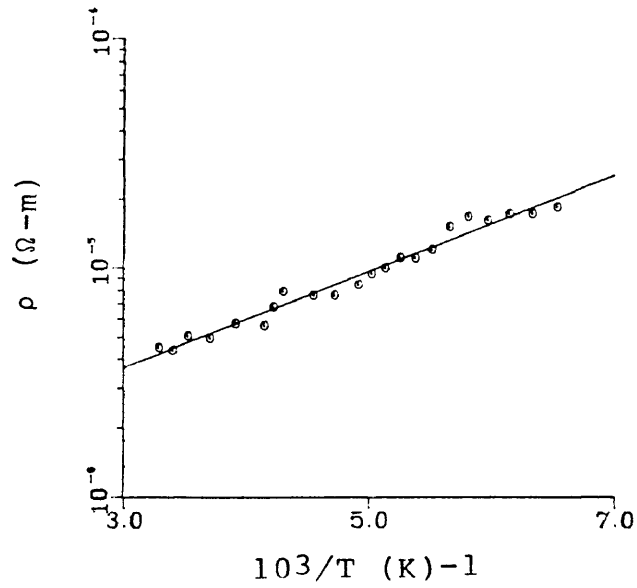


Figure 7. Resistivity of annealed antimony vs.  $103/T$ .

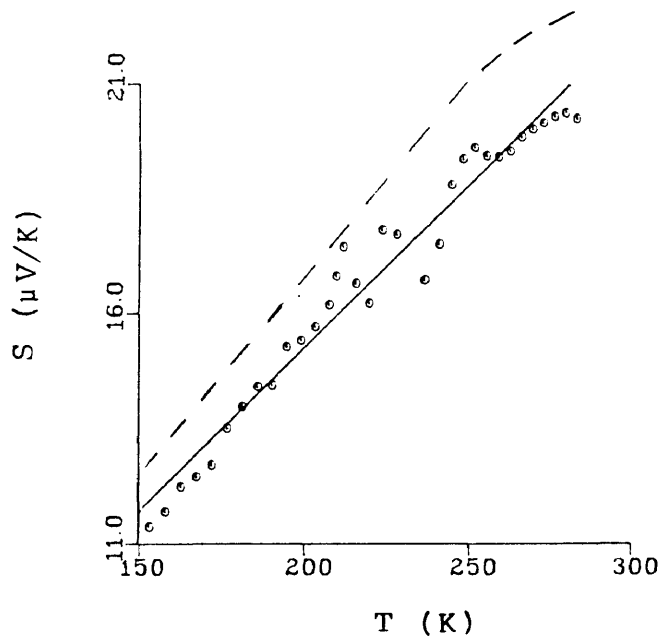


Figure 8. Thermopower of annealed antimony vs. temperature.

## B. Tellurium.

Figure 9 shows the total resistivity measured for tellurium films vs.  $T^{-1/4}$ . Figures 10 and 11 show the same data as Figure 9, but with the necessary consideration of  $R_{Sh}$ . Figure 10 is a plot of resistivity vs.  $T^{-1/4}$  and Figure 11 is a plot of resistivity vs.  $10^3/T$ . The films are labeled Tel, Te2, and Te3. Tel was run with no temperature gradient applied. Te2 and Te3 had temperature differences of about 3K and 20K respectively. This figure represents a controlled experiment in which all factors, including deposition parameters, are constant except for DT, although the thickness of Te2 varied from the other two. The value of  $R_{Sh}$  measured for Tel,  $26G\Omega$ , was not used because it was the same as the maximum value of  $R_t$  for Tel and would imply an infinite resistivity for that point. Instead an  $R_{Sh}$  of  $36G\Omega$  was used in calculations of Tel to enhance the data.

The resistivity of all three films followed the same general pattern. Starting from low temperature  $\rho$  decreased with temperature until it reached a relative minimum,  $T_{min}$ , increased until it reached a relative maximum,  $T_{max}$ , then decreased with temperature, and finally plummeted at the crystallization point,  $T_{cry}$ . These specific temperature points all shifted to higher temperatures as DT increased. The summary of these results is in Table 1.

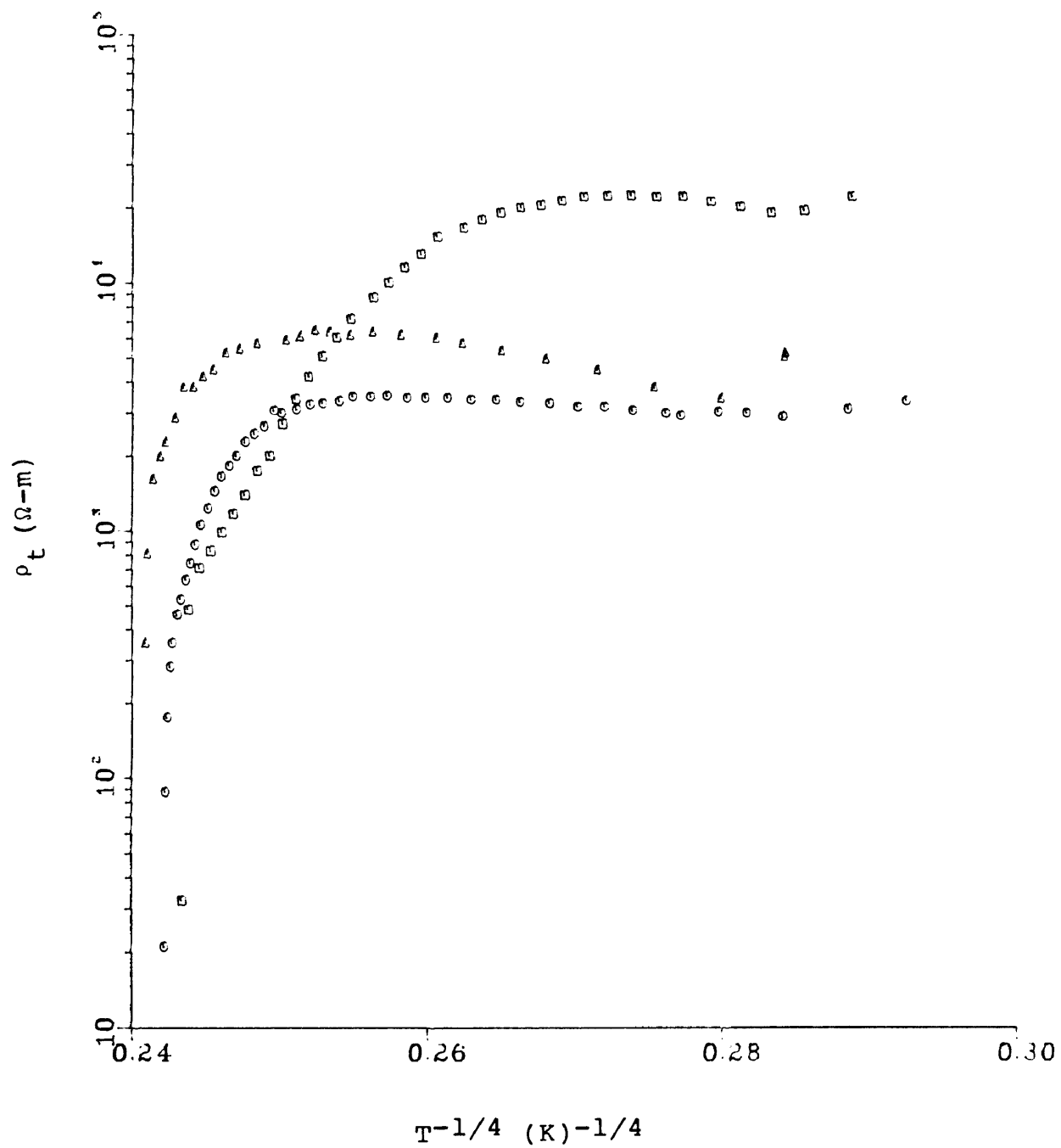


Figure 9. Total resistivity of tellurium vs.  $T^{-1/4}$   
(square - Te1, circle - Te2, triangle - Te3).

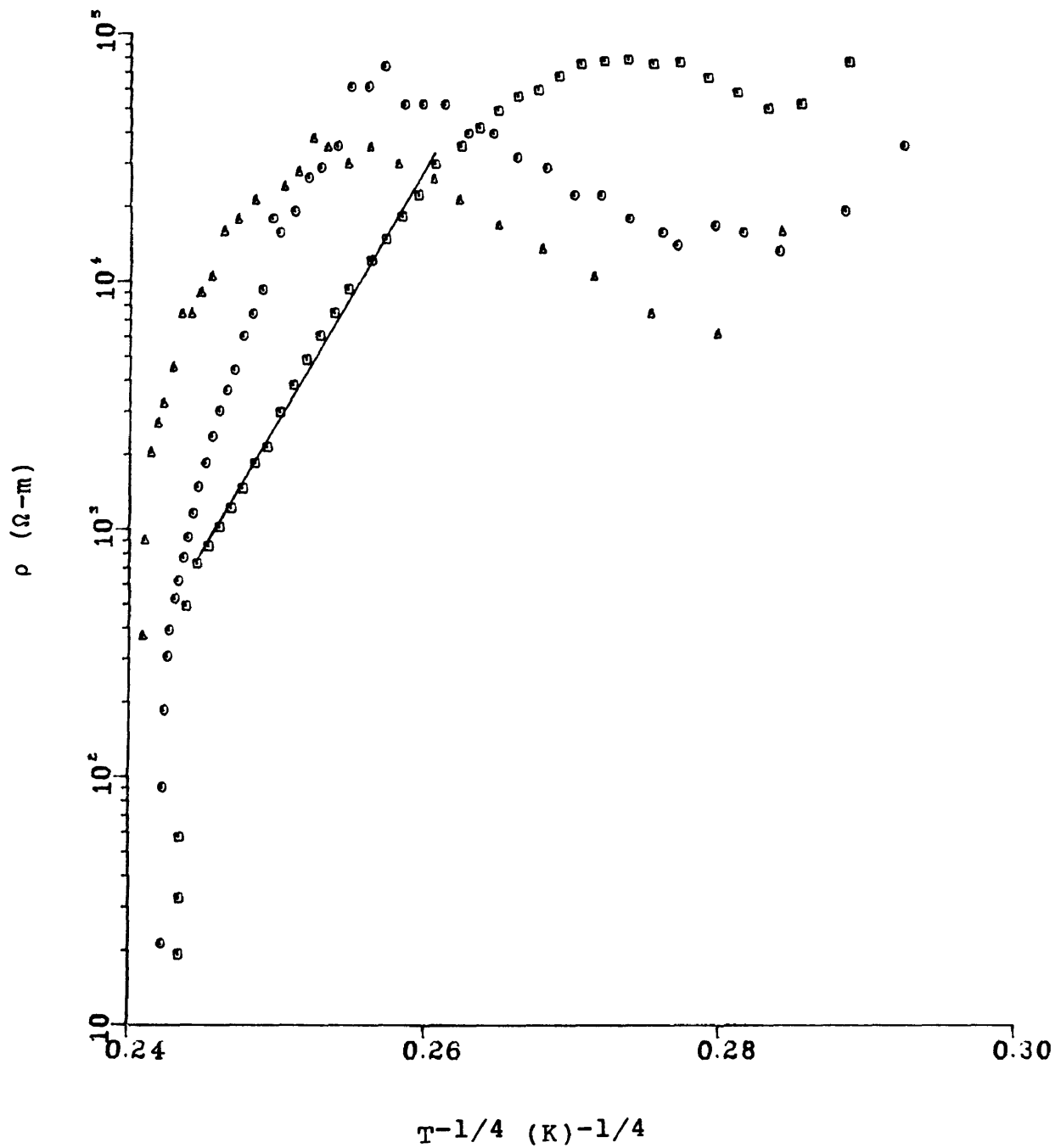


Figure 10. Resistivity of tellurium vs.  $T^{-1/4}$   
(square - Tel, circle - Te2, triangle - Te3).

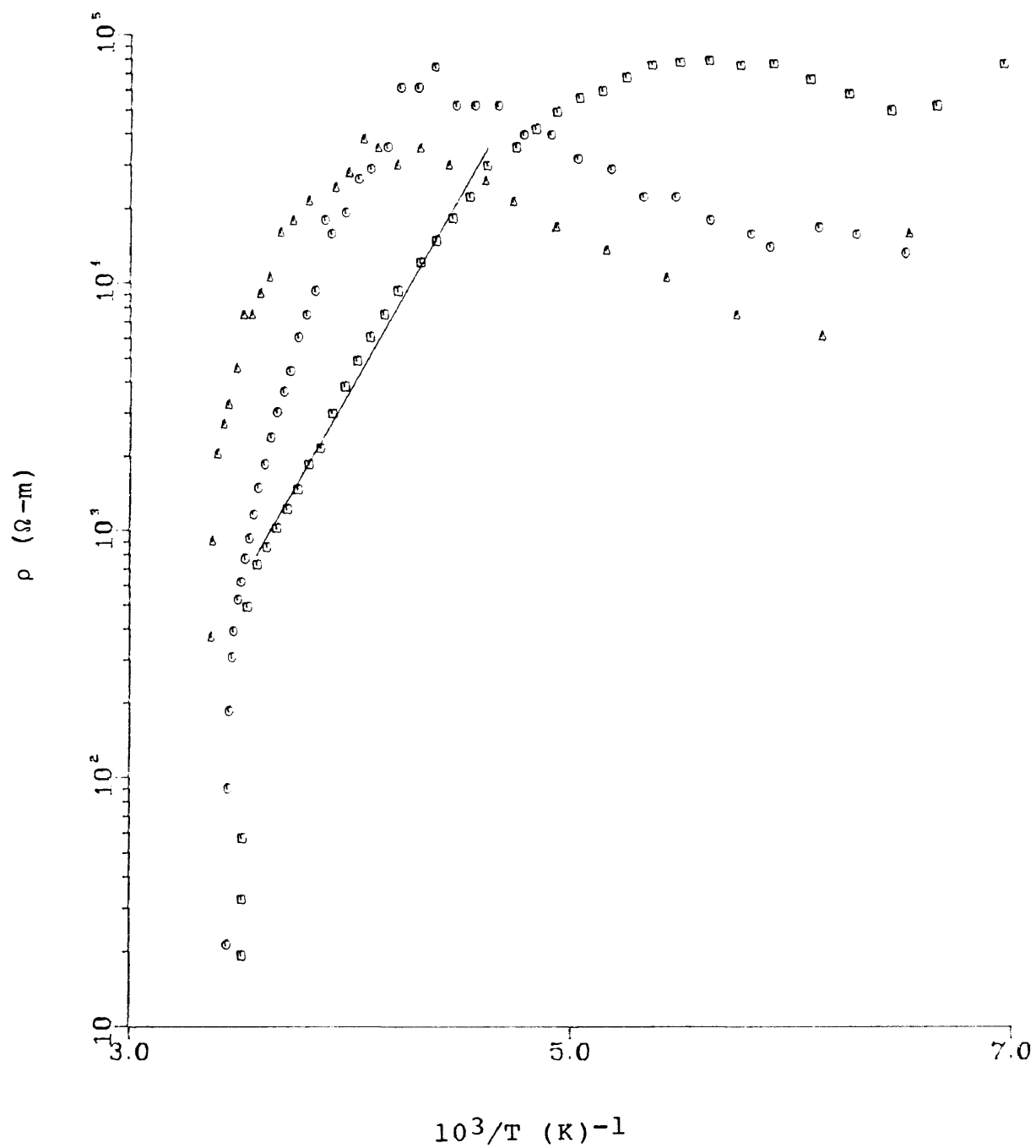


Figure 11. Resistivity of tellurium vs.  $10^3/T$   
(square - Te1, circle - Te2, triangle - Te3).

TABLE 1.  
DT, thickness,  $T_{\min}$ ,  $T_{\max}$ ,  $T_{\text{cry}}$ , and  $R_{\text{sh}}$  of tellurium.

	DT(K)	Thickness( $\text{\AA}$ )	$T_{\min}$ (K)	$T_{\max}$ (K)	$T_{\text{cry}}$ (K)	$R_{\text{sh}}$ (G $\Omega$ )
Tel	0	4360	153	184	282	36
Te2	3	1870	155	229	288	10.5
Te3	20	4780	163	247	294	9.2

For Tel it is obvious that  $R_{sh}$  was not independent of temperature. In the low temperature region, where  $R_t$  is highest, the error in the value of  $R$  caused by the incorrect assumption that  $R_{sh}$  is independent of temperature may be in excess of one order of magnitude for all samples. It is even possible that the trend observed in the temperature dependence of  $R$  is due to a trend in the temperature dependence of  $R_{sh}$ .

The plot of Tel is the most appropriate one to compare to theoretical predictions because this was the only film of uniform temperature. Figures 10 and 11 show a linear region from a point above  $T_{max}$  to a point just below  $T_{cry}$ . The values of  $T_0$  and activation energy from these plots are  $3.0 \times 10^9$  and .63eV respectively. The value for  $T_0$  is unusually large and casts some doubt on the possibility of conduction by hopping. The activation energy for this plot is much larger than the activation energy for crystalline tellurium, discussed below. This difference in activation energy can be explained by small polaron hopping. Just as in the case for antimony, it cannot be decided from this plot exactly which mechanism(s) took place.

The non linear region of the plot cannot be explained by variable range hopping or extended state conduction, but indicates there is some other method of conduction present.

The entire plot of resistivity would follow the prediction for conduction by small polaron hopping remarkably well, except that the observed  $T_{\max}$  is more than twice what the theory predicts since the Debye temperature of tellurium is only 153K.<sup>(5)</sup>

These results differ from those reported by A.M. Phale. Phale reported variable range hopping for amorphous tellurium films from 77K to a crystallization temperature of 219K and a  $T_0$  of  $6 \times 10^6$  K. The range of resistivities reported by Phale are within one order of magnitude of those reported here.<sup>(4)</sup>

Figure 12 is a plot of the thermoemf of Te3 vs. DT. Every 15 minutes the heater voltage was increased and the thermoemf was measured. The slope of the plot is  $400 \mu\text{V/K}$  and represents the average thermopower of the sample from 110-130K. This plot also represents yet another attempt at the calibration of the measurement of DT. If the thermopower was independent of temperature and the DT measurement was perfectly calibrated, then the x-intercept of this plot should be 0K, but in fact it is -28K. This value is much greater than what was measured in the other calibration measurement, but agrees in sign.

Figures 13 and 14 are plots of thermopower vs. temperature for Te2 and Te3 respectively. The two plots follow

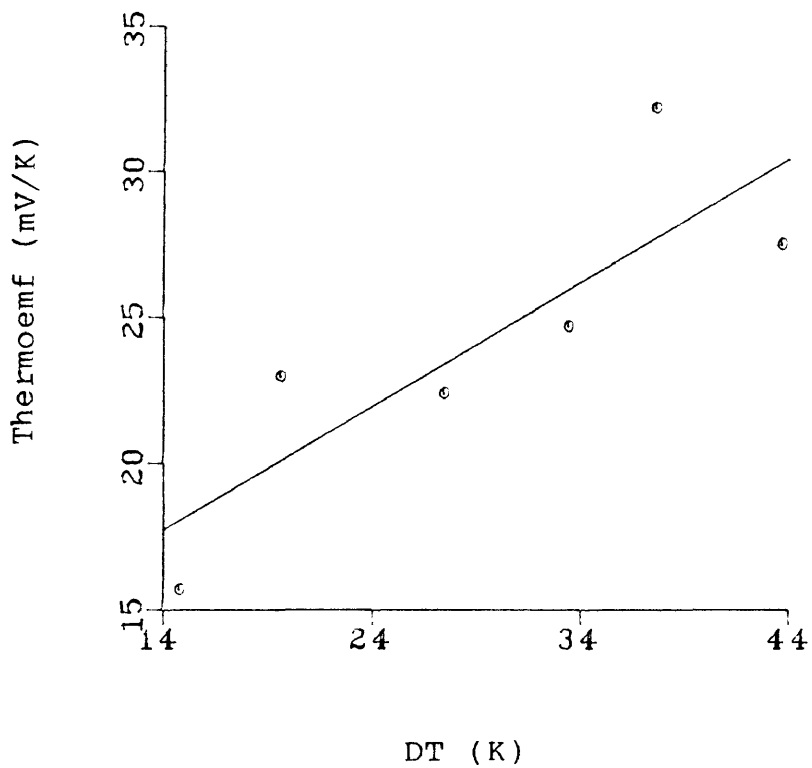
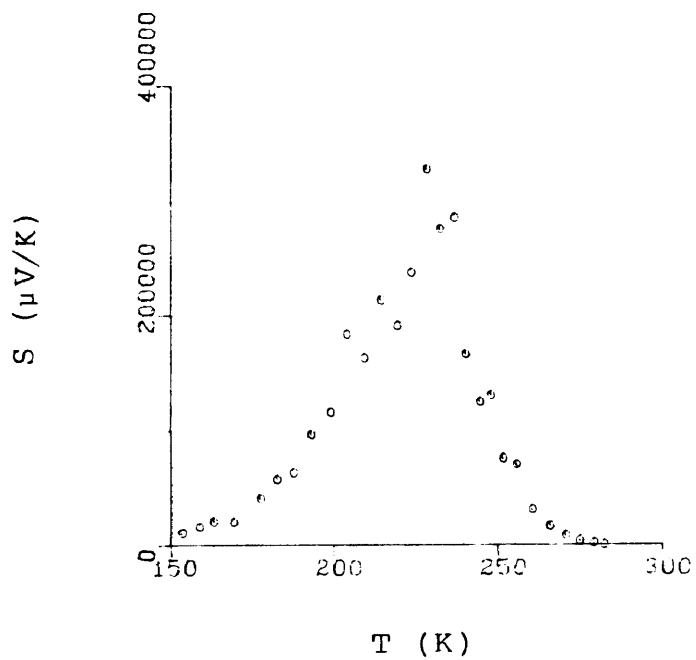
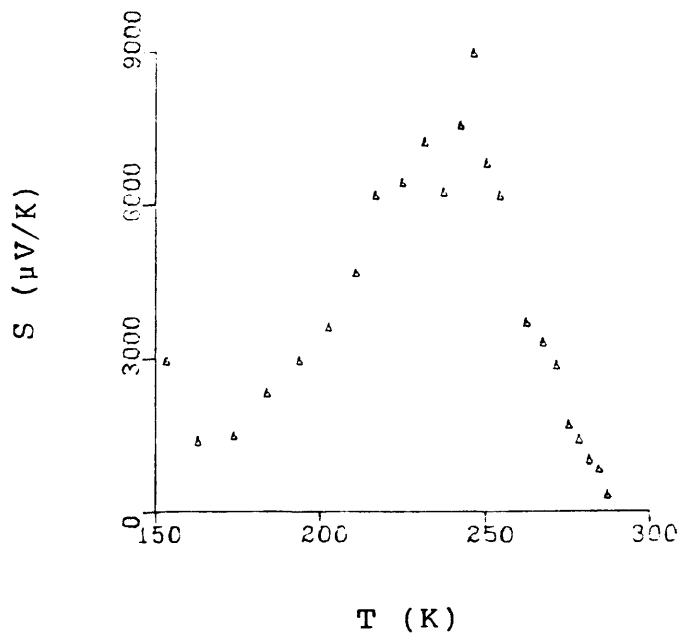


Figure 12. Thermoemf of Te3 vs. DT.

Figure 13. Thermopower of  $\text{Te}_2$  vs.  $T$ .Figure 14. Thermopower of  $\text{Te}_3$  vs.  $T$ .

similar trends, but the values of thermopower for Te2 are unreasonably large for at least two reasons. First, DT was measured as 3K for Te2, but according to the calibration attempts DT was probably a few times larger than this. Also, the measurement of I for Te2 was taken after only six minutes of relaxation. Since the measured value of I decreased as relaxation time increased, the value measured for Te2 was too large. For similar reasons, the reported values of thermopower for Te3 are probably also too high, but should be accurate to within an order of magnitude in the high temperature region.

The two plots are lambda shaped with a discontinuity in the slope at 229K for Te2 and 247K for Te3. These are the same values as  $T_{\max}$  for these samples. The thermopower is positive for all samples.

Figures 15 and 16 are plots of thermopower vs.  $10^3/T$  for Te2 and Te3 respectively. Assuming the low temperature slope is determined by the equation for  $S_e$  and that the high temperature slope is determined by the equation for  $S_h$  yields activation energies of 3.2 and 15eV respectively. These values are unreasonably large and imply that the assumptions which led to them are incorrect. The thermopower behavior also cannot be explained by variable range hopping theory since the magnitude of the thermopower is too

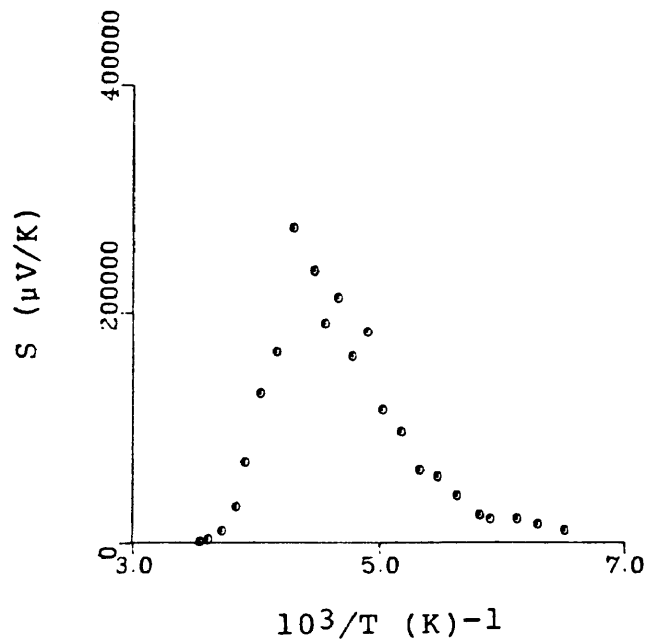


Figure 15. Thermopower of  $\text{Te}_2$  vs.  $10^3/T$ .

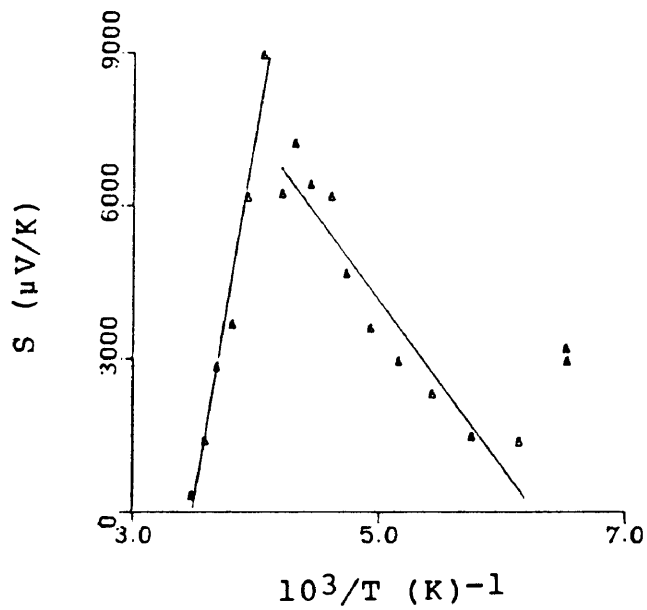


Figure 16. Thermopower of  $\text{Te}_3$  vs.  $10^3/T$ .

large. The thermopower behavior possibly may be due to a temperature dependent trapping mechanism.

Figure 17 is a plot of the resistivity of annealed, polycrystalline tellurium films vs.  $10^3/T$ . Te<sub>2</sub> was measured in situ and is called annealed Te<sub>2</sub>. Te<sub>2</sub> was later measured after being exposed to atmosphere and is called oxidized Te<sub>2</sub> because tellurium is known to oxidize upon exposure to atmosphere.<sup>(10)</sup> Also measured was a 4400 Å film evaporated while the substrate was held at room temperature called Te<sub>4</sub>. This film was also measured after exposure to atmosphere.

The plot of Te<sub>2</sub> is linear with negative slope and has a spike at 227K where resistivity increases more than one order of magnitude. The temperature of this peak is close to the value of  $T_{max}$  for amorphous Te<sub>2</sub>. DT for the measurement of annealed Te<sub>2</sub> was about the same as DT for amorphous Te<sub>2</sub>. The plot of oxidized Te<sub>2</sub> is linear with a positive slope. The activation energy of oxidized Te<sub>2</sub> is .063eV. The plot of Te<sub>4</sub> has a magnitude which is a few times smaller than the magnitude of the plot of oxidized Te<sub>4</sub>. The activation energy of Te<sub>4</sub> is .074eV.

These results differ from that reported by other authors for polycrystalline Te films. A. Goswami and S.M. Ojha reported extrinsic behavior at temperatures below 100K

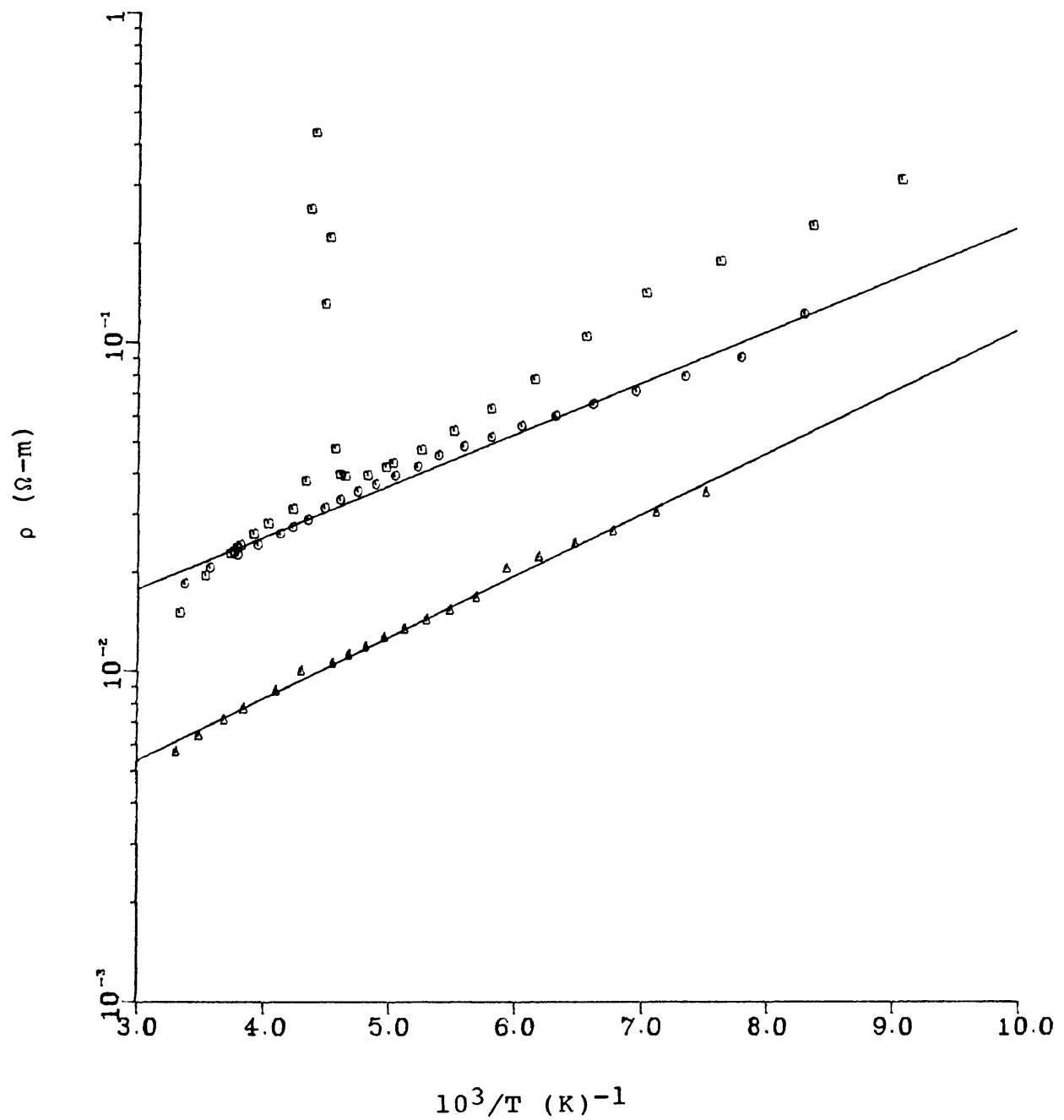


Figure 17. Resistivity of annealed tellurium vs.  $10^3/T$  (square - annealed  $\text{Te}_2$ , circle - oxidized  $\text{Te}_2$ , triangle -  $\text{Te}_4$ ).

and intrinsic behavior at temperatures above 200K. Goswami and Ojha evaporated films at substrate temperatures of 27°C and 120°C. They found intrinsic and extrinsic activation energies of .18 and .01eV respectively for the substrate temperature of 27°C. They also found intrinsic and extrinsic activation energies of .12 and .01eV respectively for the substrate temperature of 120°C.(8) The one activation energy reported here is closest to the intrinsic activation energy reported by Goswami and Ojha for the substrate temperature of 120°C.

Figure 18 is a plot of thermopower vs.  $10^3/T$  for the same films as shown in Figure 17. The thermopower of Te<sub>2</sub> increases with temperature, changes from negative to positive as the temperature passes 227K, and has a sharp dip at this temperature. This is the same temperature as the temperature of the peak of the resistivity of Te<sub>2</sub>. That the peak of resistivity and the sign change of thermopower occur at the same temperature is not surprising. As a material changes from n-type to p-type, the Fermi level may move from below mid gap to above mid gap. At mid gap, the activation energy is a maximum, and thus, so is the resistivity. The plot of oxidized Te<sub>2</sub> is linear with negative slope at low temperatures and saturates at high temperature. If the slope of the linear region is assumed to follow the equation

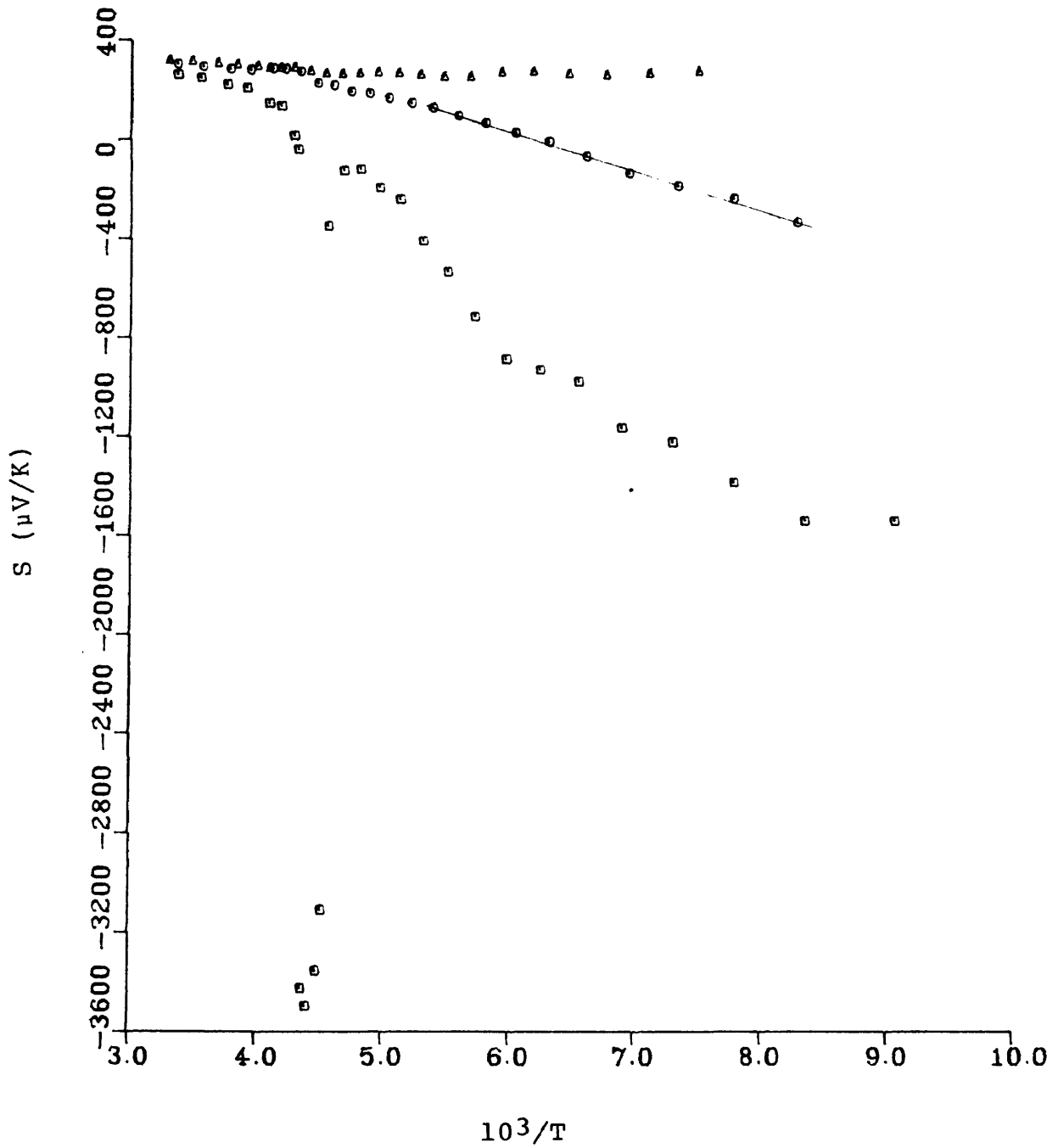


Figure 18. Thermopower of annealed tellurium vs.  $10^3/T$  (square - annealed Te<sub>2</sub>, circle - oxidized Te<sub>2</sub>, triangle - Te<sub>4</sub>).

for  $S_e$ , then the activation energy for oxidized Te2 is .030eV. Unlike the other two plots, the plot of Te4 decreases gradually with temperature in the low temperature region. It then increases slowly with the temperature. All three plots converge at about 300  $\mu$ V/K at room temperature.

The results given by S. Chaudhari et al. for thermopower of polycrystalline tellurium films agree most closely with the plot of oxidized Te2, but have a steeper slope in the linear region.

Figure 19 is a scanning electron micrograph of annealed oxidized Te2, with a magnification of 20,000x. Only a portion of the film is shown, of course, but the film had uniform appearance across its entire length and width when viewed with the electron microscope. The average grain size, if that is a word which can be used to describe this polycrystalline film, is about 6000  $\text{\AA}$ . The grain boundaries are diffuse with thin regions between the grains. The surface is strewn with microcracks of length varying from a couple of thousand angstroms to a few microns. This non-percolating microcrack structure explains why the resistivity of annealed Te2 is higher than the resistivity of Te4. As seen by the naked eye, the film appeared shiny and uniform.

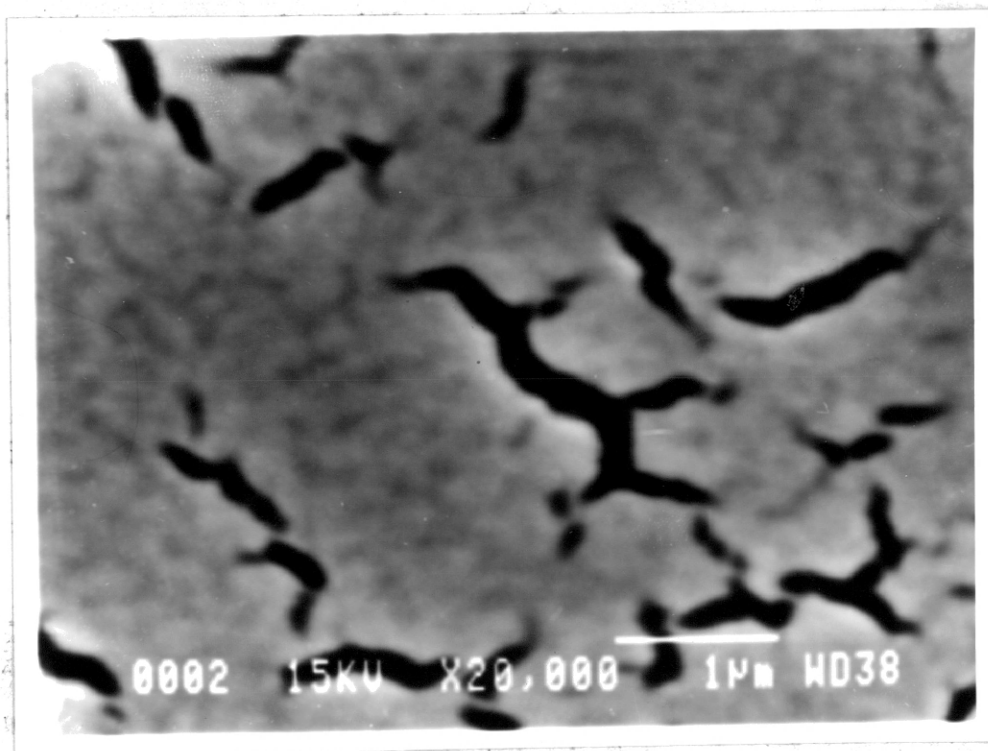


Figure 19. Electron Micrograph of Annealed Te2.

There is evidence that these microcracks formed upon crystallization. As  $\text{Te}_3$  crystallized, its resistivity dropped nearly to the typical room temperature level and then increased sharply and irreversibly. This film had a network of percolating microcracks that was visible with the naked eye. Hauser looked at amorphous antimony films and the same films after annealing with an electron microscope. He saw that the annealed films had microcracks but did not see any microcracks in the amorphous films, indicating the microcracks formed upon annealing.(3)

A possible explanation of the appearance of annealed tellurium is as follows. The amorphous film was of a very uniform thickness, due to the rapid lowering of the adatoms' speed as they hit the cold substrate surface upon deposition. During crystallization, many of the atoms redistributed themselves slightly relative to their neighboring atoms. The new bond lengths were shorter, on the average, than the previous bond lengths. Thus, the film shrank upon annealing, producing both the thin regions between grains and the microcracks as well, because the glass substrate did not shrink so abruptly.

Figure 20 is a scanning electron micrograph of  $\text{Te}_4$  with a magnification of 20,000x. Grains of the polycrystalline film appear round or oblong in shape with a width of about

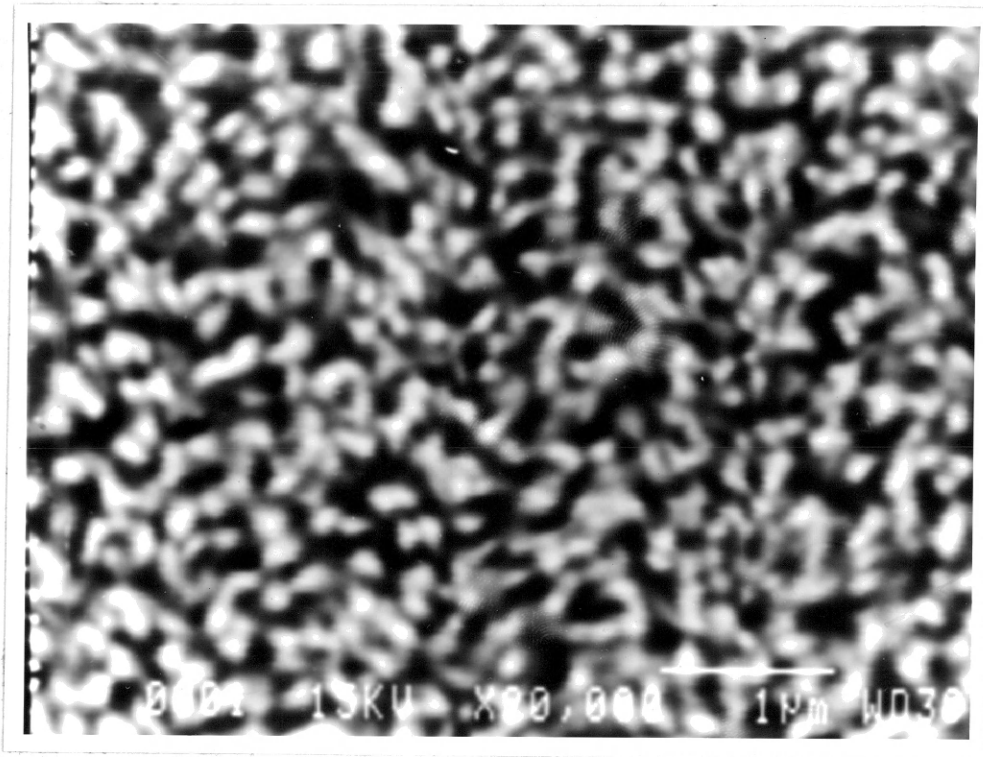


Figure 20. Electron Micrograph of Te4.

2000 Å. The grains are interconnected into a percolating network, as is evidenced by the finite resistivity of the film. X-ray diffraction spectrographs of both films, not shown here, indicate the c-axis of the tellurium crystals lies parallel to plane of the substrate. As viewed by the naked eye, the film appeared darker and less shiny than annealed Te<sub>2</sub>.

B. Chakrabati et al. displayed electron micrographs and X-ray diffraction spectra of polycrystalline tellurium films evaporated at substrate temperatures ranging from room temperature to 200°C. They found that all films had a c-axis orientation parallel to the plane of the substrate. Also, they found that all films evaporated at substrate temperatures up to 150°C had a needle-shaped structure, and films evaporated at a substrate temperature of 200°C had structures like that shown here for Te<sub>4</sub>.(12)

A possible reason for this discrepancy is as follows. The crucible used for this experiment was cylindrical and has parallel walls unlike the common crucible shape, which has walls that flute outward. Chakrabati et al. did not specify the shape of their crucible, and the present argument assumes they had a common variety. Before the evaporated tellurium atoms left the cylindrical crucible, they passed through a region with a relatively high density of

tellurium vapor and formed clusters of atoms. Upon impact with the substrate, the clusters broke apart any delicate needle-shaped clusters which may have begun to form.

## V. SUMMARY

The goals established for this project were achieved. A technique of preparing uniform amorphous tellurium films was developed. Order of magnitude measurements of the resistivity and thermopower of these films were made.

The resistivity and thermopower of amorphous tellurium, annealed polycrystalline tellurium, amorphous antimony, and annealed polycrystalline antimony films were measured from 120K - 320K. The behavior of resistivity and thermopower of the amorphous films could be explained by extended state conduction, variable range hopping, nearest neighbor hopping, or small polaron conduction, but it was impossible to conclusively decide which of these mechanism(s) actually took place.

The need for a number of future projects was established. The measurement system within the vacuum chamber should be rewired so that  $R_{sh}$  is at least  $10^{12}\Omega$ . In order to accomplish this it may be necessary to modify the actual design of the sample holder since a possible source of finite shunt resistance is between the heat sinks and the copper probes. Either an electrometer which can make faster measurements of current and resistance should be acquired or these measurements should be recorded at periodic time

intervals while they relax and their time saturated values carefully estimated. Each thermocouple should be reconnected with its copper probe so that the thermocouple junction itself is entirely imbedded within its probe. The thermocouples should then be calibrated for temperature measurement.

## REFERENCES CITES

1. N.F. Mott and E.A. Davis, Electronic Processes in Non-Crystalline Materials, 2nd ed., Oxford (1979).
2. J.J. Hauser, Phys. Rev. B 9, 2623 (1974).
3. D.S. Peters, Thermoelectric Properties of Amorphous Sb and Te, Colorado School of Mines, T2530 (1981).
4. A.M. Phale, Thin Solid Films 61, L21 (1979).
5. Charles Kittel, Introduction to Solid State Physics, 5th ed., New York (1976).
6. D. De, C.K. Ghosh, and A.K. Pal, Thin Solid Films 110, 193 (1983).
7. A. Boyer, D. Desahacht, and E. Groubert, Thin Solid Films 76, 119 (1981).
8. A. Goswami and S.M. Ojha, Thin Solid Films 16, 187 (1973).
9. J.M. Ziman, Electrons and Phonons, Oxford (1961).
10. A. Nussbaum and R.J. Hager, Phys. Rev. 123 No. 6, 1958 (1961).
11. S. Chaudhari, B. Chakrabarti, and A.K. Pal, Thin Solid Films 82, 217 (1981).
12. B. Chakrabarti, S. Chaudhari, G.L. Malhotra, and A.K. Pal, J. Appl. Phys. 51 No. 8, 4111 (1980).